

# Development of the Skewed Rotation Plane (SRP) Waist Joint for Humanoid Robots

Robert W. Ellenberg  
Drexel University  
rwe24@drexel.edu

Richard Vallett  
Drexel University  
rjv35@drexel.edu

R. J. Gross  
Drexel University  
rjg48@drexel.edu

Brittany Nutt  
Drexel University  
brittany.nutt@drexel.edu

Paul Y. Oh  
Drexel University  
pyo22@drexel.edu

**Abstract**—As humanoid robotics advances beyond bipedal walking, complex motions involving the whole body are necessary. Most recent humanoids represent the range of motion of the human spine with a single rotation joint. While this joint allows the body to swing during dynamic walking, any bending must be performed only with the legs. This paper develops a skewed rotation plane (SRP) waist joint to give a humanoid robot the same range of torso motion as a human. The SRP design reduces holding torque compared to a orthogonal-axis joint. An inverse kinematics solver using Jacobian Pseudo-inverse was developed to produce smooth torso orientation trajectories. Finally, a mechanical prototype developed and fitted to Drexel University's Jaemi Hubo to verify and validate the model.

## I. INTRODUCTION

Traditionally, humanoid robots have a slightly simplified body plan compared to that of humans. Robots such as the Hubo KHR4 [1], HRP-2 [2], and ASIMO<sup>1</sup>, for example, all have 6 degrees of freedom in each leg, 7 in each arm, and a single rotary joint at the waist, connecting the upper and lower bodies. While the kinematics of these arms and legs give similar ranges of motion to human arms, the waist joints of many humanoids do not match the range of motion of the human torso [3] (Table I). For locomotion research such as dynamic walking [4], [1], the torso's primary role was to compensate for angular momentum of the legs during walking.

More challenging locomotion problems, such as uneven terrain or stair-climbing, a fully-articulated upper body becomes useful to help stabilize the robot. In [5], an HRP-2 humanoid was shown to walk over sloped surfaces, while grasping a hand-rail. The stable region, and the range of possible walking trajectories, was shown to be significantly larger when holding a handrail. With a single-DOF waist, however, the humanoid was limited in how far it can reach to grasp the handrail.

Robots that lack a multi-DOF torso must move many more joints to tilt the torso. For example, a robot such as the Hubo2 must bend forward at the hip joints to tilt forward, and actually bend one or both legs to tilt sideways (Figure 2). These restrictions can reduce the range of motion when the robot must reach over a tall obstacle (Figure 1). A multi-DOF torso can bend around the obstacle, allowing an arm to reach farther past the edge. Using leg joints to tilt the robot

can also make planning whole-body motions more difficult, since lower body tasks (balance, foot placement) and upper body tasks (manipulation) are more coupled. More recent

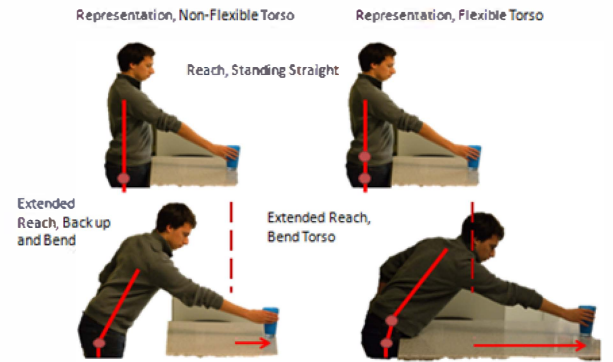


Fig. 1. A human bending from the back (left) can reach forward over an obstacle, where bending from the hips (right) would cause a collision.

humanoid research has focused on a whole-body locomotion and manipulation [6], [7]. In general these tasks require higher-level planning to satisfy the many constraints imposed by the task. Methods based on Rapidly-Exploring Random Trees (RRT) [8], for example, can plan motions to satisfy multiple, simultaneous task-based constraints [9]. In this case, additional DOFs give the planner freedom to explore for solutions that would over-constrain a simpler robot. Particularly for service

Left Lateral Bending	50°
Right Lateral Bending	50°
Flexion (Front)	45°
Extension (Back)	30°
Right Rotation	40°
Left Rotation	40°

TABLE I. RANGE OF MOTION FOR A TYPICAL HUMAN SPINE.

robotics, many humanoid designs have appeared that have more than one DOF in the waist joint. For example, the iCub [10] uses a 3-DOF differential drive joint, allowing the waist to achieve similar bend angles to a human waist, while in [11], a 2 DOF differential drive gives a similar range of motion to a YiREN mobile robot. In [12], a humanoid robot was developed with a “double spherical” joint, which allowed the legs to effectively rotate about a single center point. The Rollin’ Justin

<sup>1</sup><http://asimo.honda.com/>

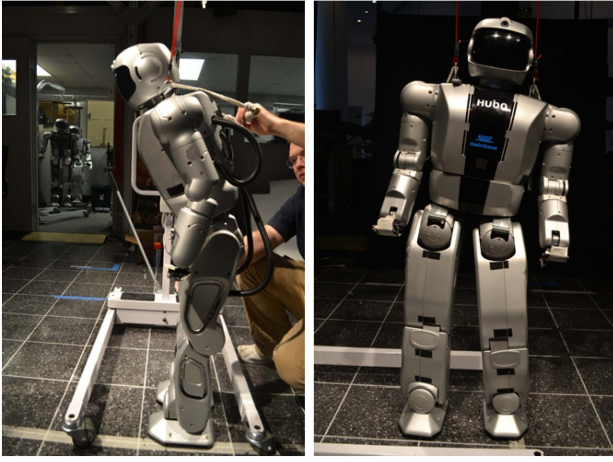


Fig. 2. Pitching the torso of the KAIST Hubo2 Humanoid (left) requires bending at the hips. (Right) Roll side-to-side requires significant bending at the knees to tilt the hips.

[13] uses an active/passive combination of joints to provide yaw (twist) and pitch motion for the torso. [14] develops a humanoid robot with a 3-DOF yaw-pitch-roll joint, showing a range of motion similar to the human back. The HRP4<sup>2</sup> has a 2DOF orthogonal joint that allows side-to-side tile motion. Almost all of these joint designs use orthogonal axes that directly tilt the torso in each direction. While simple to model, orthogonal axes require each actuator to directly support the weight of the upper body when tilted.

This paper presents a design for a humanoid robot waist: the Skewed Rotation Plane (SRP) joint (Figure 3), a compact, joint to approximate the range of motion of the human waist. The joint design was inspired by joints found in atmospheric diving suits<sup>3</sup>, where joints must sustain high pressures without buckling. Similar kinematics are also found in robots such as the Kinova Jaco<sup>4</sup>, though to the authors knowledge, the design has not previously been implemented as a waist joint. The main contributions of this paper are:

- 1) The SRP joint is shown theoretically and experimentally in Section II to match or exceed the range of motion of the typical human torso.
- 2) A Jacobian-Pseudoinverse Inverse Kinematics solver is developed in Section III, and is experimentally shown to solve arbitrary torso rotation trajectories.
- 3) Improvements in energy consumption are explored in Section IV, showing reduced motor torque at large tilt angles.

## II. KINEMATICS AND REACHABILITY

The SRP joint in general is an arrangement of three or more joint axes that are tilted a small angle  $\theta_b$  from each other (Figure 3). Unlike the orthogonal axes of traditional Roll-Pitch-Yaw (RPY) gimbals, the SRP joint axes have  $\theta_b \ll 90^\circ$

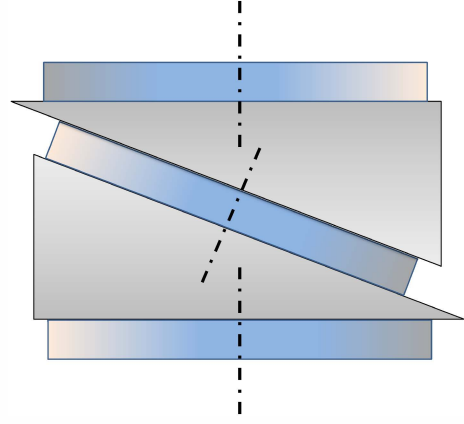


Fig. 3. The simplest SRP joint consists of three rotation axes. Each body in the joint has a rotation axis, tilted at an angle of  $\theta_b$  to the previous body.

between each body. The sequence of rotations from the fixed base to the end of the joint can be derived from this angle and each of the joint angles  $\theta_j, j \in \{1, 2, 3\}$ , the rotation of the  $j^{th}$  joint axis. The final orientation of the joint is given (1) where  $R_i(\theta), i \in \{x, y, z\}$  represents a rotation by  $\theta$  about the  $i^{th}$  coordinate axis. This is commonly known as the extrinsic formulation.

$$R = R_z(\theta_1)R_y(-\theta_b)R_z(\theta_2)R_y(\theta_b)R_z(\theta_3) \quad (1)$$

Rotating each joint segment has the effect of precessing the next joint axis. By setting  $\theta_b$  to be identical for the first  $n - 1$  joints, maximum precession  $\psi_{max}$  is achieved when each segment is rotated  $180^\circ$  with respect to the previous segment. This can be shown analytically by considering the relationship between this maximum overall bend angle of the torso,  $\psi_{max}$ , and the Torso's  $\hat{k}$  vector. The  $3^{rd}$  component of the Torso's  $\hat{z}$  vector is found by expanding (1), resulting in (2). The maximum precession / bend is therefore the maximum angle between the  $\hat{z}$  and  $\hat{k}$  vectors, which is related to  $R_{3,3}$  by (2). The minimal value of  $R_{3,3}$  occurs when  $\psi_2 = \pi$  in (4). Using the half-angle identity, the maximum value is shown to be  $2\theta_b$ .

$$R_{3,3} = 1 - 2\sin^2\left(\frac{\psi_2}{2}\right)\sin(\theta_b)^2 \quad (2)$$

$$\cos(\psi_{max}) = \underset{\psi_2}{\operatorname{argmin}}(R_{3,3}) \quad (3)$$

$$\cos(\psi_{max}) = 1 - 2\sin^2(\theta_b) = \cos(2\theta_b) \quad (4)$$

Finally, the rotation introduced by the last joint,  $R_z(\psi_3)$ , is identical to the yaw motion of the last joint of the RPY joint  $\gamma$ . Therefore, within the mechanical limits of the joint, any reasonable desired yaw is possible. Note that this yaw rotation is about the local  $\hat{z}$  axis. Together, these limits (4) bound the SRP joint's kinematic reachability.

The reachable space was also established by a sampling method over all possible joint angles. Sampling randomly from  $[0, 2\pi]$  for each joint angle produces a random torso orientation  $R_s$  for the SRP joint. This rotation matrix can be expressed in the equivalent pose of an RPY joint by by extracting an

<sup>2</sup><http://global.kawada.jp/mechatronics/hrp4.html>

<sup>3</sup><http://www.oceanworks.com/hsCommercial.php>

<sup>4</sup><http://kinovarobotics.com/products/jaco-research-edition/>

equivalent combination of  $\alpha, \beta$ , and  $\gamma$  that represents  $R$ . The Tait-Bryan angles  $\alpha$  about the x-axis,  $\beta$  about the y-axis, and  $\gamma$  about the z-axis can be determined from the components of  $R$ . If condition (5) is imposed, then the conversion in [15] can be simplified to (6).

$$\alpha, \beta, \gamma \in \left(-\frac{\pi}{2}, \frac{\pi}{2}\right) \quad (5)$$

$$\begin{aligned} \beta &= \text{asin}(R_{1,3}) \\ \alpha &= \text{atan2}\left(\frac{R_{2,3}}{\cos(\beta)}, \frac{R_{3,3}}{\cos(\beta)}\right) \\ \gamma &= \text{atan2}\left(\frac{R_{1,2}}{\cos(\alpha)}, \frac{R_{2,2}}{\cos(\alpha)}\right) \end{aligned} \quad (6)$$

The choice of the number of DOF and  $\theta_b$ , should ideally achieve the same range of motion as the human spine.  $\theta_b$  must be large enough to accommodate extension, flexion, and lateral rotation in Table I. This constraint is given in (7), resulting in a minimum  $\theta_b$  of  $23^\circ$ . Sampling 10,000 random orientations resulted in the reachability space of Figure 4. Each point represents a tuple of the Tait-Bryan angles. The roll-pitch view includes the subset of points such that  $\gamma \in \left(-\frac{\pi}{2}, \frac{\pi}{2}\right)$ .

$$\theta_b > \frac{\max(\theta_f, \theta_r)}{2} \quad (7)$$

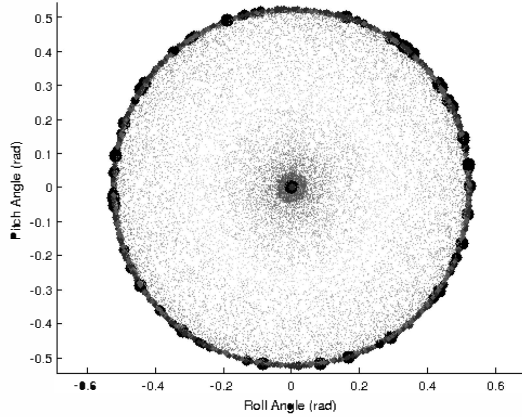


Fig. 4. The reachability space of the 3-DOF SRP joint. The size of the markers is proportional to the condition estimate  $\log_{10}(C)$

An important concern in the design of non-orthogonal joints like the RPY joint is the manipulability of the joint over its range of motion. Kinematic manipulability, explored in [16], relates the ability of a manipulator to move an end effector in a task space. For a typical 7-DOF robotic arm, the task space consists of three Cartesian dimensions and three orientation dimensions, or a 6-DOF space. A kinematic singularity occurs when a manipulator cannot create a differential movement in one or more directions in the task space. Manipulability is essentially a measure of the condition of the constraint

Jacobian. For an  $m \times n$  Jacobian Matrix, the condition  $C$  is given in (8).

$$C = \frac{\sigma_1}{\sigma_m} \quad (8)$$

As the ratio  $C$  becomes larger, the manipulability grows poorer: essentially, some task-space motions require large changes in joint angles. Figure 4 shows a region of poor manipulability near the origin, as well as at the edge of the reachable space. While increasing  $\theta_b$  and soft-limiting the range of motion can avoid the  $2^{nd}$  region, it is impractical to simply avoid the origin, as this is often the home position for a humanoid robot. By introducing an extra initial bend by  $\theta_b$ , however, this singularity can be shifted away from the origin (9). The resulting reachability of this modified configuration is shown in figure 5. While the singular region is not eliminated in this case, it can be placed outside the nominal range of motion. This result makes the SRP-style of joint uniquely suited to a waist joint's small range of motion. In a robotic arm that requires rotations of on the order of  $180^\circ$ , it becomes impractical to avoid this singularity.

$$R_{new} = R_y(-\theta_b)R \quad (9)$$

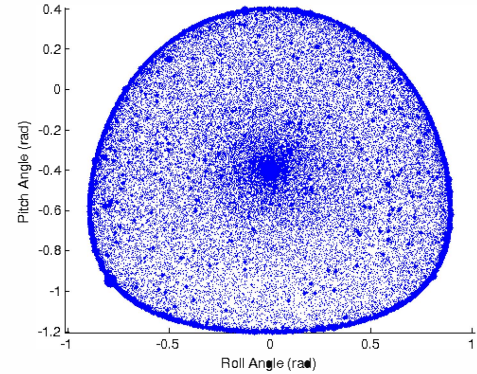


Fig. 5. An initial tilt of the joint shifts the singular region away from the equilibrium pose

Another way to mitigate the kinematic singularity is to add an additional degree of freedom to the joint. Figure 6 shows two alternative configurations for the additional DOF. The resulting ranges of motion for each case are shown in figure 7. The additional DOF does not remove the central singularity, and in the case of the second modification, introduces an additional singular region. Increasing the number of joints does increase the overall reachability. If the joint is constrained to only positive pitch angles, the operating region becomes singularity-free. To achieve full range of motion, the Torso can simply be mounted at a fixed angle. When the torso is rotated forward to be level, the joint will be pitched forward.

These reachability spaces for the 3 DOF and 4 DOF designs show mixed but promising results. All tested designs show at least one near-singular region within the reachable space,



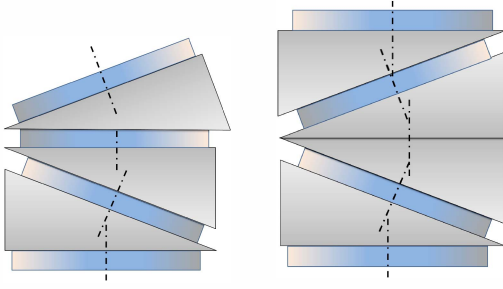


Fig. 6. (Left) An additional DOF is added in between the 2nd and 3rd joints of the basic design. (Right) The additional DOF is added at the end of the kinematic chain

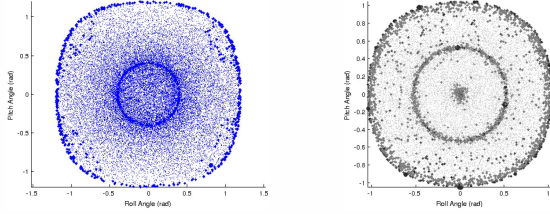


Fig. 7. Reachability plot for 4 DOF designs. Both plots show regions of near-singularity within the reachable space.

requiring that the IK solver be able to cope with these regions. However, by reducing the operating region in software, the desired range of motion can still be achieved while also avoiding these problematic regions.

### III. INVERSE KINEMATICS SOLVER

Recalling that the limits of the human torso are significantly less than  $90^\circ$  of rotation in roll, pitch, and yaw, we claim the following:

- 1) For “human-like” torso rotations, it is sufficient to constrain the possible rotations of the SRP joint to  $\pm 90$  deg in any direction.
- 2) This reduced space of rotations is uniquely parameterized by 3 components of the rotation matrix.

Based on human anatomy, the typical humanoid coordinate system has its x axis pointing forward from the torso, the y axis to its left, and the z axis upwards through the head. These directions are perpendicular to the standard anatomical planes: the coronal, sagittal, and transverse planes, respectively. In particular, the transverse plane, or X-Y plane, divides  $\mathbb{R}^3$  into half-spaces. Recalling the maximum pitch and roll of the torso (table I, the  $\hat{z}$  vector of the torso is never rotated farther than  $45^\circ$  from the Hip’s  $\hat{K}$  axis. Thus, the vector is constrained to lie in the positive half-space defined by  $R_{3,3} > 0$ . Given the unit magnitude of  $\hat{z}$ , the constraint (10) implies that its x and y components will uniquely determine the vector.

$$\sqrt{1 - \hat{k}_x^2 - \hat{k}_y^2} = \hat{k}_z = 1, z \in (0, 1] \quad (10)$$

A half-space constraint is also imposed on the  $\hat{x}$  basis vector, constraining the yaw angle  $\gamma$ . Thus, one additional parameter

is sufficient to specify the y vector: its z component. The third unit vector is trivially found from the cross product of the first two. Therefore,  $R_{21}$ ,  $R_{31}$ , and  $R_{32}$  form a possible constraint vector.

$$\hat{k}j = 0$$

$$\hat{j}_y = \sqrt{1 - \hat{j}_x^2 - \hat{j}_z^2} \quad (11)$$

These constraints are not intuitive, however, so it is desirable to specify the desired orientation constraints with conventional Tait-Bryan angles. A trivial answer is to simply compare the joint rotation matrix  $R$  directly with the desired rotation matrix given in (13). Unfortunately, the gradient of each term in the rotation matrix is not conducive to numerical solution if a given component is close in magnitude to 1. A small rotation in any direction will tend to reduce the magnitude of the rotation at this point.

A better way is to use the desired orientation as an inverse rotation.  $R_l b$  is transposed and left-multiplied to the joint rotation matrix  $R$ . When a set of joint angles is a solution, this overall rotation matrix  $R_c$  given in (12) is approximately the identity matrix.

$$R_c = R_{lb}^T R \quad (12)$$

$$R_{lb} = R_\alpha R_\beta R_\gamma \quad (13)$$

Because only off-diagonal terms are specified in the constraints, the three constraints are zero at the solution. These off-diagonal terms are also nicely formulated in terms of their gradient: a small displacement of rotation in any direction is expressed well in the constraints (14).

$$C = \begin{pmatrix} \cos(\theta) \sin(\phi) \\ \sin(\theta) \\ \cos(\theta) \sin(\psi) \end{pmatrix} \quad (14)$$

Taking the Jacobian (15) shows that the constraints are decoupled in the local neighborhood of the solution. This formulation can then be used with numerical Jacobian Pseudo-Inverse methods to find inverse kinematics solutions.

$$J \Big|_{\vec{0}} = \begin{pmatrix} 0 & 0 & 1 \\ 0 & -1 & 0 \\ 1 & 0 & 0 \end{pmatrix} \quad (15)$$

To solve inverse kinematics of the joint, a Jacobian Pseudo-Inverse solver was developed in MATLAB. Because of the relatively low number of DOFs, the constraints were directly formulated as a sequence of rotation matrices, such as in (1). The three constraint terms developed in II are functions of the joint angles, the wedge bend angle  $\theta_b$ , and the desired orientation angles  $\alpha$ ,  $\beta$ , and  $\gamma$ . In this formulation, the bend angle and desired angles are treated as constant parameters. The Jacobian of these constraints with respect to the joint variables is calculated symbolically, then stored as a function. Thus, the Jacobian at an arbitrary position can be exactly evaluated simply by calling this function.

Once a goal orientation is chosen, (16) is iteratively evaluated until the orientation error is below a specified tolerance.

$$\begin{aligned}\Delta\vec{\psi} &= J_r \vec{\psi}^+ \Delta\vec{p} \\ \vec{\psi} &= \vec{\psi}_0 + \Delta\vec{\psi}\end{aligned}\quad (16)$$

#### IV. MOTOR TORQUE

Under static loading, the SRP joint is advantageous over the RPY joint in that it requires less motor torque to support a given pose. Because the joint axes are oriented along the body, much of the torque applied due to pitching or rolling the torso,  $\vec{\tau}$ , is supported directly by reaction forces in the mechanism. Simplifying the torso to a lumped-mass approximation, the load applied to the waist during a static pose is given in (17), where  $m$  is the mass of the upper body and  $\vec{c}$  is the center of mass position with respect to the Torso frame of reference.

$$\vec{\tau} = R\vec{c} \otimes m\vec{g} \quad (17)$$

The load torque can then be projected onto each motor axis to estimate the required motor torque to hold that pose in (18), where  $\tau_j$  is the motor torque for joint  $j$ , and  $\hat{z}_j$  is the  $z$  unit vector for the  $j^{th}$  joint segment. If the torso is assumed to be a centered lumped mass, then  $\vec{c}$  reduces to  $[0, 0, c_z]^T$ . Similarly, the theoretical static load for the equivalent RPY joint can be calculated by projecting the load torque onto the roll, pitch, and yaw axes. Since current is proportional to torque at stall in a DC motor, and assuming identical motors, the sum of motor torques is an equivalent measure to the sum of motor currents. Therefore, a given joint's operating cost  $f$  can be characterized by (19).

$$\vec{\tau}_j = \vec{\tau} \cdot \hat{z}_j \quad (18)$$

$$f = \sum_j |\tau_j| \quad (19)$$

To show the torque savings of the SRP joint, the minimum holding torques were calculated for every pose in the reachability space constructed previously. The ratio of the cost  $f$  to that of the RPY joint is shown in figure 8. At most, the SRP joint requires 39% of the torque that an RPY joint requires, and the mode is only 27.5%.

#### V. PROTOTYPE DESIGN

The design for the mechanical prototype is based on the 3DOF concept introduced in section II. Shown in Figure 9, this design has a notable change: The top half of the middle body is rotated  $90^\circ$  about the vertical axis with respect to the bottom half. This rotation has the effect of moving the joint singularity from the origin (Figure 10). The singularity present at the origin has become an unreachable region of diameter  $11.5^\circ$  centered at  $\alpha = 0.26rad, \beta = 0.0rad$ . The shaded region shown represents the convex region of pitch and roll angles in which there is no joint singularity. Table II summarizes the physical properties of the prototype (Figure 11). All parts of the frame were machined from  $8mm$ , 6061-T6 plate stock on a Tormach PCNC-1100 CNC milling machine. The three harmonic drives (labeled) are connected to the 200W Maxon Brushless Motors

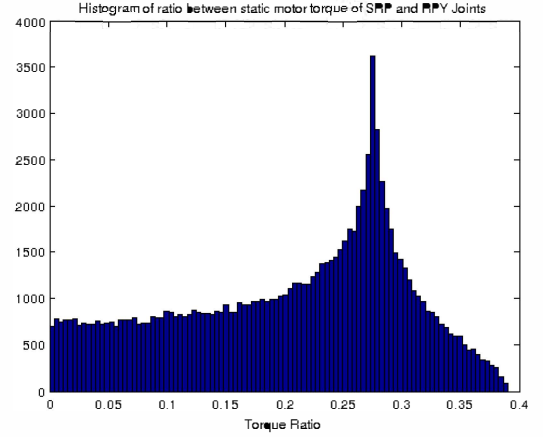


Fig. 8. Total torque cost as a fraction of the equivalent RPY joint, for positions in the reachability space.

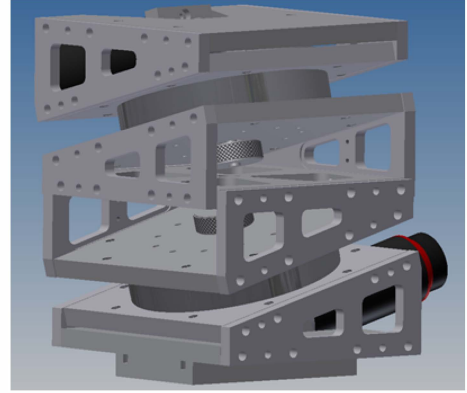


Fig. 9. Modified SRP joint with a  $90^\circ$  rotation offset between the 2nd and 3rd joints.

via a set of 32-tooth,  $0.5mm$  module miter gears. The miter gears allowed the motors to be mounted perpendicular to the drive axes. This reduces the space required between the joints, which is essential in reducing the height of the mechanism.

The completed prototype (Figure 11) has been mounted to a Hubo2 torso. Using two Hubo motor controllers, the prototype was able to actuate through the range of motion. Future iterations of this design will focus on weight and size reduction. Good candidates for size reduction include using

TABLE II. PROPERTIES OF SRP JOINT MECHANICAL PROTOTYPE

Length	10cm
Width	10cm
Height	13.2cm
Mass	3kg
Roll Range	$\pm 36.1^\circ$
Pitch Range	$-10.0^\circ, +22.1^\circ$
Maximum Joint Velocity	$270 \frac{deg}{sec}$
Drive Motor (3)	Maxon 200W, 314176
Gear Reduction (3)	Harmonic Drive SHD-20-160-2SH 32 tooth, 0.5mm module $45^\circ$ miter gear

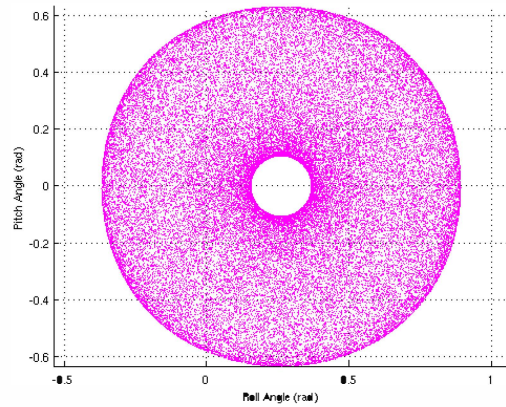


Fig. 10. The modified design shows an unreachable region of approximately  $11.5^\circ$  centered at  $\alpha = 15^\circ, \beta = 0^\circ$ .

smaller harmonic drives and thinner structural plates to reduce weight.

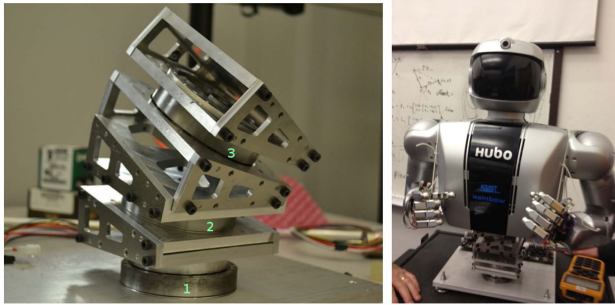


Fig. 11. Prototype design assembled on test fixture with joint angles of  $15^\circ$ ,  $90^\circ$ , and  $90^\circ$ .

## VI. CONCLUSIONS

This paper demonstrated a waist joint design for the Hubo2 humanoid robot that provides a range of motion similar to a human. Kinematic simulation showed that collision-free, arbitrary trajectories were possible throughout the specified range of the joint. A simple modification was also demonstrated that moved the kinematic singularity outside the range of motion. The full-scale prototype was then developed and implemented to verify and validate the design. Plate manufacturing techniques allowed the design to be made with 2.5D machining methods, reducing machining time associated with complex 3D joints.

## REFERENCES

- [1] I.-W. Park, J.-Y. Kim, and O. Jun-Ho, "Online biped walking pattern generation for humanoid robot khr-3(kaist humanoid robot - 3: Hubo)," in *Humanoid Robots, 2006 6th IEEE-RAS International Conference on*, 2006, pp. 398–403.
- [2] K. Kaneko, F. Kanehiro, S. Kajita, H. Hirukawa, T. Kawasaki, M. Hirata, K. Akachi, and T. Isozumi, "Humanoid robot hrp-2," in *Robotics and Automation, 2004. Proceedings. ICRA '04. 2004 IEEE International Conference on*, vol. 2, 26–may 1, 2004, pp. 1083 – 1090 Vol.2.

- [3] A. S. Romer and T. S. Parsons, *The Vertebrate Body*, T. S. Parsons, Ed. Philadelphia, PA: Holt-Saunders International, 1977.
- [4] S. Kajita, F. Kanehiro, K. K., Y. K., and H. H., "The 3d linear inverted pendulum mode: a simple modeling for a biped walking pattern generation," in *Intelligent Robots and Systems, 2001. Proceedings. 2001 IEEE/RSJ International Conference on*, vol. 1, 2001, pp. 239–246 vol.1.
- [5] K. Harada, M. Morisawa, M. K., N. S., F. K., K. K., and K. S., "Kinodynamic gait planning for full-body humanoid robots," in *Intelligent Robots and Systems, 2008. IROS 2008. IEEE/RSJ International Conference on*, 2008, pp. 1544–1550. [Online]. Available: <http://dx.doi.org/10.1109/IROS.2008.4650862>
- [6] N. Vahrenkamp, D. Berenson, T. Asfour, J. Kuffner, and R. Dillmann, "Humanoid motion planning for dual-arm manipulation and re-grasping tasks," in *Intelligent Robots and Systems, 2009. IROS 2009. IEEE/RSJ International Conference on*, oct. 2009, pp. 2464 –2470.
- [7] A. Dietrich, T. Wimbock, A. Albu-Schaffer, and G. Hirzinger, "Reactive whole-body control: Dynamic mobile manipulation using a large number of actuated degrees of freedom," *IEEE Robotics & Automation Magazine*, vol. 19, no. 2, pp. 20–33, June 2012.
- [8] S. M. LaValle, "Rapidly-exploring random trees: A new tool for path planning," Iowa State University, Tech. Rep., 1998. [Online]. Available: <http://msl.cs.uiuc.edu/lavalle/papers/Lav98c.pdf>
- [9] D. Berenson, J. Chestnutt, S. Siddharth, K. James, and K. Satoshi, "Pose-constrained whole-body planning using task space region chains," in *IEEE-RAS International Conference on Humanoid Robots (Humanoids09)*, 2009.
- [10] W. Hinojosa, N. Tsagarakis, G. Metta, F. Becchi, G. Sandini, and D. Caldwell, "Performance assessment of a 3 dof differential based waist joint for the "icub" baby humanoid robot," in *Robot and Human Interactive Communication, 2006. ROMAN 2006. The 15th IEEE International Symposium on*, sept. 2006, pp. 195 –201.
- [11] Z. Tiejun, T. Dalong, and Z. Mingyang, "The development of a mobile humanoid robot with varying joint stiffness waist," in *Mechatronics and Automation, 2005 IEEE International Conference*, vol. 3, 2005, pp. 1402 –1407 Vol. 3.
- [12] G. Li, Q. Huang, Y. Tang, G. Li, and M. Li, "Kinematic analysis and motion planning of a biped robot with 7-dof and double spherical hip joint," in *Intelligent Control and Automation, 2008. WCICA 2008. 7th World Congress on*, june 2008, pp. 2982 –2987.
- [13] M. Fuchs, C. Borst, P. Giordano, A. Baumann, E. Kraemer, J. Langwald, R. Gruber, N. Seitz, G. Plank, K. Kunze, R. Burger, F. Schmidt, T. Wimboeck, and G. Hirzinger, "Rollin' justin - design considerations and realization of a mobile platform for a humanoid upper body," in *Robotics and Automation, 2009. ICRA '09. IEEE International Conference on*, may 2009, pp. 4131 –4137.
- [14] A. Omer, Y. Ogura, H. Kondo, A. Morishima, G. Carbone, M. Ceccarelli, H. ok Lim, and A. Takanishi, "Development of a humanoid robot having 2-dof waist and 2-dof trunk," in *Humanoid Robots, 2005 5th IEEE-RAS International Conference on*, dec. 2005, pp. 333 –338.
- [15] G. Slabaugh, "Computing euler angles from a rotation matrix," Georgia Institute of Technology, Tech. Rep., August 1999. [Online]. Available: <http://www.gregslabaugh.name/publications/euler.pdf>
- [16] F. Park and J. W. Kim, "Manipulability and singularity analysis of multiple robot systems: a geometric approach," in *Robotics and Automation, 1998. Proceedings. 1998 IEEE International Conference on*, vol. 2, may 1998, pp. 1032 –1037 vol.2.